2023

# Experimental and Analytical Studies of Size Effects on Compressive Ductility Response of Ultra- High-Performance Fiber-Reinforced Concrete

Md. Habibur Rahman Sobuz

Arafat Alam

Deric John Oehlers

Phillip Visintin

Adbul Hamid Sheikh

*See next page for additional authors*

Authors
Md. Habibur Rahman Sobuz, Arafat Alam, Deric John Oehlers, Phillip Visintin, Adbul Hamid Sheikh, Mohamed Ali Sadakkathulla, and Michael Griffith

Published (2023) Construction and Building Materials, 409, art. no. 133864

# Experimental and Analytical Studies of Size Effects on Compressive Ductility Response of Ultra-High-Performance Fiber-Reinforced Concrete

[1]Md. Habibur Rahman Sobuz*, [2]Arafat Alam, [3]Deric John Oehlers, [4]Phillip Visintin, [5]Adbul Hamid Sheikh, [6]Mohamed Ali Sadakkathulla and [7]Michael Griffith

*Corresponding Author:
[1]Dr. Md. Habibur Rahman Sobuz
Assistant Professor
Department of Building Engineering and Construction Management
Khulna University of Engineering and Technology
Khulna 9203, BANGLADESH
and
Former Research Fellow
School of Civil, Environmental and Mining Engineering
The University of Adelaide
South Australia 5005, AUSTRALIA
E-mail: habib@becm.kuet.ac.bd

[2]Arafat Alam
Graduate Research Assistant
Department of Civil and Environmental Engineering, University of Nebraska-Lincoln, Peter Kiewit Institute, Omaha, NE 68182, USA

[3]Dr. Deric John Oehlers
Emeritus Professor
School of Civil, Environmental and Mining Engineering
The University of Adelaide
South Australia 5005, AUSTRALIA

[4]Dr. Phillip Visintin
Associate Professor
School of Civil, Environmental and Mining Engineering
The University of Adelaide
South Australia 5005, AUSTRALIA

[5]Dr. Abdul Hamid Sheikh
Associate Professor
School of Civil, Environmental and Mining Engineering
The University of Adelaide
South Australia 5005, AUSTRALIA

[6]Dr. Mohamed Ali Sadakkathulla
Senior Lecturer
School of Civil, Environmental and Mining Engineering
The University of Adelaide
South Australia 5005, AUSTRALIA

[7]Dr. Michael Griffith
Professor
School of Civil, Environmental and Mining Engineering
The University of Adelaide
South Australia 5005, AUSTRALIA

**Experimental and Analytical Studies of Size Effects on Compressive Ductility Response of Ultra-High-Performance Fiber-Reinforced Concrete**


## Abstract

Ultra-high-performance fiber-reinforced concrete (UHPFRC) has gained a great deal of increasing interest in structural engineering applications, particularly where high ductility, strength, and high impact resistance are of prime concern. This study focuses primarily on the size effects ductility characteristics of UHPFRC with varying fiber concentrations subjected to uniaxial compressive load. It shows how to process the data from compression cylinder tests to extract the size-dependent strain at peak stress to provide a generic size-dependent stress-strain analytical model. Furthermore, a numerical flexural segmental moment-rotation approach is applied to incorporate an analytical model to quantify apparently disparate UHPFRC member strength and ductility. Tests have shown that it is not the enhancement in the material concrete compressive strength but the phenomenal brittle ductility nature, observed as a result of increasing the slenderness of the specimen; in contrast, a substantial increase in ductility was achieved after crushing of concrete due to the addition of fibers. A size-dependent analytical approach has estimated good fit with the experimental and other published results. Finally, numerical simulation using a segmental approach at the ultimate limit state of rotation dealing with flexural ductility is significantly influenced by the increase in slenderness factor of the specimens and fiber concentrations.



**Keywords:** UHPFRC; Size effects; Stress-strain relationship; Fiber concentration; Ductility, Slenderness factor.


## 1 Introduction

The quick advancement of infrastructure has increased demand for concrete and consequently created opportunities for the newer generation of concrete. For this purpose, new types of concrete have been pioneered in the construction industry with high mechanical performance such as high-strength concrete (HSC) and fiber-reinforced concrete (FRC). Ultra-High-Performance Concrete (UHPC), a new type of innovative new-generation cementitious concrete composites that was created in the past ten years. To create Ultra-High-Performance Fiber-Reinforced Concrete (UHPFRC), steel fibers are typically combined with cement matrix in UHPC. UHPFRC exhibits improved Young's modulus, tensile strength, post-cracking flexural and ductility responses [1, 2]. UHPFRC can achieve compressive strengths in the range of 120 MPa - 800 MPa by intricately blending reactive constituents and utilizing novel curing techniques [3-6].

Previously, efforts had been made to comprehend the variables that affected the compressive behaviors of UHPFRC. Even without complex mixing and exorbitant materials, it can easily achieve a compressive strength of around 160 MPa [1, 7]. The mechanical characteristics involving uniaxial compressive, tensile, and ductile responses are enumerated basic material properties for RC member design, and these behaviors of UHPFRC can be improved using various high-strength discontinuous short fibers or by blending with micro and macro fibers [8-13]. To appraise structural responses, measuring the complete stress-strain behaviors of the UHPFRC specimens under monotonic compression is required. Limited work has been attempted to evaluate the overall compressive stress-strain and ductility behaviors through the intrinsic test setup with the platen-to-platen deformation measurement under concentric loading [6, 14]. Hassan and Jones [15] utilized circular rings with LVDTs to measure elastic deformation, and two LVDTs were situated parallel to the specimen to measure softening behavior. Axial post-peak softening deformation was measured by Prabha and Dattatreya [16] using two LVDTs positioned between the platens on two different sides of the specimen. It is anticipated that the material stress-strain ductility behaviors of UHPFRC depend not only on the concrete's constituents, such as the quantity and type of fibers added to the mix, but also on the specimen's size, shape, and testing procedures [17]. Furthermore, the test has determined that the specimen strength significantly varies when the length-to-width ratio is greater than two, indicating that the strength is highly size-dependent. Consequently, the specimen under maximum stress and the corresponding softening branch decreases with length and depends on the size factor. It could be attributed to the various zones of behavior on the specimens connected to compression failure and researcher-recognized methods like energy to quantify the large deformations for compression behavior of specimens [18]. Therefore, the primary influencing factor that may regulate the overall stress-strain behaviors of UHPFRC is the size effects resulting from different sizes of specimens. Different specimen sizes and shapes have been used to determine the stress-strain response of identical materials, with different degrees parameters [19]. To quantify the effect of fibers, Kazemi and Lubell [20] found that peak strengths and softening behavior in compression, flexure, and direct shear strength also increased as the content of fibers increased. This phenomenon is explained by the ability of steel fibers to allow for more significant axial deformation while partially restricting lateral expansion. Kazemi and Lubell [21] demonstrated that the materials part of the stress-strain curve has a linear slope independent of fiber concentration. However, it has been noted in the works of other researchers that, beyond a certain point, an increased quantity of steel fibers contributes to fiber merging, creating weak spots that can lower fiber quality and, as a result, lower compressive strength [22, 23]. Compressive strength and ductility significantly decrease with increasing specimen slenderness factor ($\mu = L_{pr}/d_{pr}$, the ratio of length to diameter or width of the specimen) according to numerous studies [20, 24-26]. This suggests that the specimen's higher slenderness factor showed brittle behavior compared to its lower slenderness factor, but no clear relationship has been established, and more research is required regarding the various specimen slenderness factors, fiber concentrations, and corresponding post-peak ductility responses.

Although UHPFRC test results show superior strength and ductility for material and structural members, the costly and complex production processes prevent them from having the desired effect [27]. Additionally, the repetitions of the testing for each new material need high-capacity machinery setups, large space, time, and high cost, which poses a significant obstacle to the development of new materials. To tackle this issue of analyzing the stress-strain characteristics of normal strength concrete (NSC) and HSC, many researchers have proposed numerical models with an empirical basis [28-30]. These numerical models mostly work accurately until the peak stress or the ascending branch while showing limited reasonable agreements in the softening branch. Although numerical models for the stress-strain response of NSC and HSC are available, analytical models incorporating size-effect of total stress-strain behavior for UHPFRC are still largely unavailable in the literature. The numerical model that predicts the stress-strain behavior of UHPFRC and takes size dependence characteristics into account will hasten our understanding of UHPFRC and allow us to use it in large-scale simulation using simulation software.

Ductility is crucial in allowing the member to attain its ultimate strength by absorbing higher energy. It is important to resist both seismic and blast loads and to simulate the collapse mechanism of RC structures [24, 31]. Although it is recognized that the structural behaviors and failure are anticipated to be size-dependent, concrete members are designed following the strength of standard specimen size. For instance, the capacity of a plastic hinge to rotate is size-dependent owing to concrete softening [32]. Carpinteri, and Corrado [33] proposed a size effect model incorporating the strain localization concept to predict the cracking behaviors of RC beams at the loading condition. However, their research expressed ductility as a function of reinforcement ratio and beam depth which is a progressive common phenomenon in RC members. On contrary, Hillerborg [34] suggested that the size effect is based on the localization length that can be determined from the experimental data with the best-fitting approach. Previous finding has revealed that the inclusion of fibers in UHPFRC can enhance its material ductility behavior [15] and flexural ductility capacity to rotate at the hinges region [35]. A numerical flexural segmental moment-rotation approach is appropriate to quantify the deformation-based hinge rotation of RC members incorporating the size effects phenomenon. It allows the formation of wedges at concrete softening into the analysis [36]. Significant research has been done on the rotational strength of structures made of conventional concrete, but generally speaking, the majority of the advice in the codes of practice is empirical and exhibits a sizable amount of scattered results. [37]. It is surmised that producing a conceptual mechanics-based numerical approach that well predicts the test response of the member can help to adjust and build up design rules for structural members. To quantify the size-effect response of a reinforced UHPFRC member at the hinge region, the development of a simple and efficient approach that ultimately relies on the material properties for any size of RC members with the size-dependent stress-strain material behavior will have a wide range of applications.

The key output of this paper is to study the size-dependent compressive stress-strain response of UHPFRC with varying fiber concentrations. This paper first illustrates the approach to quantifying the stress-strain response of UHPFRC and combines a large body of existing published test data to produce an analytical model that encompasses a range of UHPFRC sample sizes and fiber concentrations. The compressive stress-strain relationships are determined as a size-dependent parameter based on the test data, capturing the full softening response suitable for each RC beam size. These properties are then used in a numerical segment analysis of flexure to show how to quantify moment-rotation at the extreme limit, along with changes in bending and bending stiffness. Further, the moment-rotation section discusses the influence of fiber concentration and a sample size range encompassing all the structural mechanisms needed to fully simulate rotation along with wedge formations of the UHPFRC beam.

## 2 Experimental program

An experimental laboratory program was conducted at the University of Adelaide, South Australia. The experimentation was mainly conducted on UHPFRC cylindrical specimens with three different fiber concentrations (FC) that were included 1%, 2%, and 3% by weight of cement. It was comprised of 144 cylindrical specimens that had a fixed diameter of 100 mm, but with varying heights of 200 mm, 300 mm, and 400 mm. The concrete test specimens were designated the symbol as "Exp. D × H – F" by the following process: the first word "Exp." indicates to experimental specimen; the second set of lettering "D × H" indicates each specimen dimension with the diameter (D) and height (H), for example, the dimension of the specimen size of 100 X 200 mm in height as refer "100 × 200", and the final letter e.g. "F" refers to the fiber concentration. The influence of fiber concentration was evaluated for the slenderness factor of 2, 3, and 4, incorporating the size-dependent compressive ductility behaviors in the softening region of the UHPFRC specimens. For each specimen size and fiber concentration, four specimens were investigated under compressive loading. The mean values were considered to calculate the final stress-strain responses. It should be mentioned that the mean of the cylindrical specimen with a slenderness factor equal to 2 is considered a reference factor to evaluate the relationship between the other specimen size factors.

### *2.1 Materials, mixing, and experimental testing*

This experimental section considered the mix composition as provided in Table 1. It was based on the detailed UHPFRC mix design published in our previous research article by Sobuz, Visintin [1]. Sulphate-resisting cement considering fineness index of 365 $m^2/kg$ was used in the UHPFRC mix. The silica fume incorporating bulk density of 625 $kg/m^3$ was considered for the concrete mixture. The FM 2.34 of river sand was used in the concrete preparation in lieu of expensive silica sand. Cold-drawn hooked end wire 4D steel fibers (Dramix-BG) was incorporated in the concrete mix as illustrated in Fig. 1. The properties of steel fiber provided by the manufacturer Bekaert Ltd in South Australia are illustrated in

Fig. 1. (a) 4D steel fiber (b) Single part of fiber with 60 mm length

Table 2. Sika ViscoCrete -10 superplasticizer was used in the concrete mixture. In addition, the UHPFRC mixing procedure was followed according to the Sobuz, Visintin [1].

Table 1: Mix proportions of UHPFRC

| Material constituents ($kg/m^3$) | | | | | |
|---|---|---|---|---|---|
| Cement | Sand | Silica fume | Steel fibers | Water | Superplasticizer |
| 920 | 920 | 245 | 161 | 163 | 41.4 |

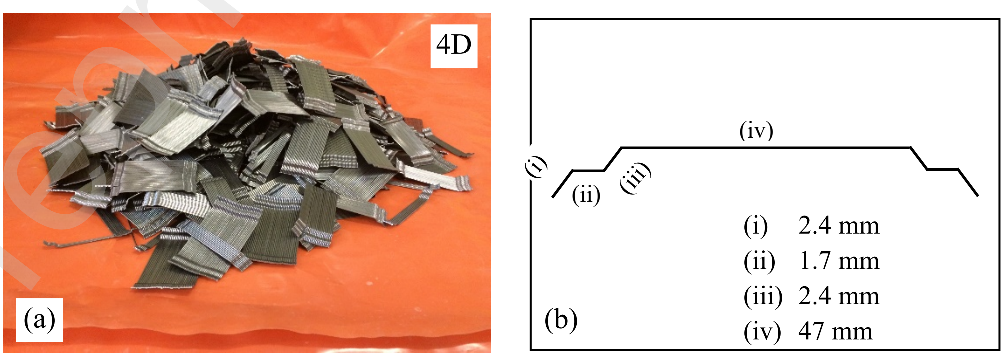

Fig. 1. (a) 4D steel fiber (b) Single part of fiber with 60 mm length

Table 2: Properties of 4D steel fiber

| Properties | 4D Fiber |
|---|---|
| Tensile strength (MPa) | 1500 |
| Young's modulus (MPa) | 210 |
| Length of fiber (mm) | 60 |
| Diameter (mm) | 0.9 |
| Aspect ratio | 66 |

For each fiber concentration from 1% to 3%, three types of cylinders with 100 mm fixed in diameter with varying heights of 200 mm, 300 mm, and 400 mm were cast in the laboratory. Afterward, all the concrete specimens were kept in a fog room prior to the test day. Before testing, each specimen's top and bottom compressive loading sides were grounded attentively to achieve a strong, level surface. All concrete specimen preparation and curing methods followed the code of standard ASTM-C31/C-31M-12 [38].

All of the specimens' compression strength and stress-strain responses were carried out by an Amsler machine rated capacity of 5000 kN at 56 day curing period complying ASTM-C39/C39M-12[39] as shown in Fig. 2. For determining the stress-strain response of the specimens, four LVDTs were equipped to determine the overall platen-to-platen contraction and three LVDTs placed equally in the lateral direction at half-length were instrumented to calculate the full lateral dilation. The rate of load was controlled at 50 kN/min in the linear branch through load control; thereafter softening branch was followed by the displacement rate at 0.1mm/min to ensure the deflection control for capturing the complete stress-strain response.

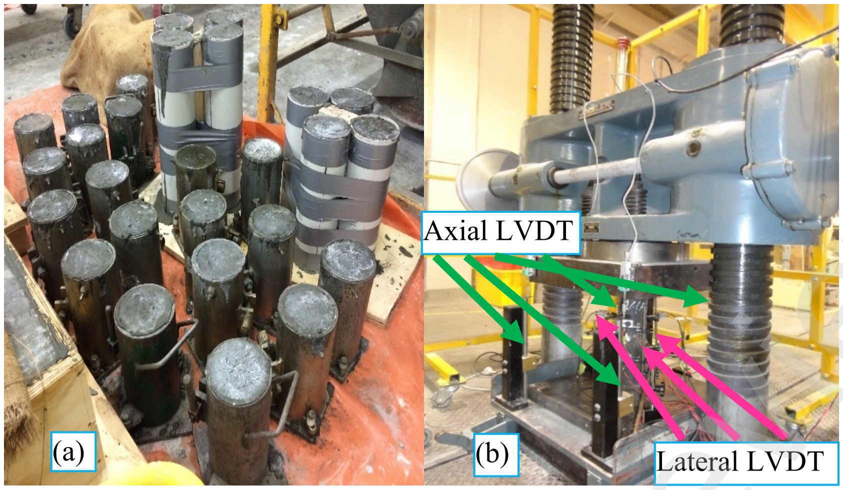


Fig. 2. UHPFRC specimens (a) preparation of varying sizes (b) typical test setup and instrumentation

# 3 Analytical program

## *3.1 Idealization of axial stress-strain response*

The stress-strain behavior of UHPFRC may be correlated when cylindrical or prismatic specimens are evaluated under concentric loading. The stress $\sigma_{ax}$ application in Fig.3 leads to an axial contraction of the specimen along the height $L_{def}$. Fig. 4 shows how axial deformation changes as applied stress changes. The ascending branch (OA) till the peak strength ($f_{cc}$) can be thought of as a linear material deformation known by the $\varepsilon_{mat}$ recorded by strain gauges. That is,

$$\delta = \varepsilon_{mat} L_{def} \qquad (1)$$

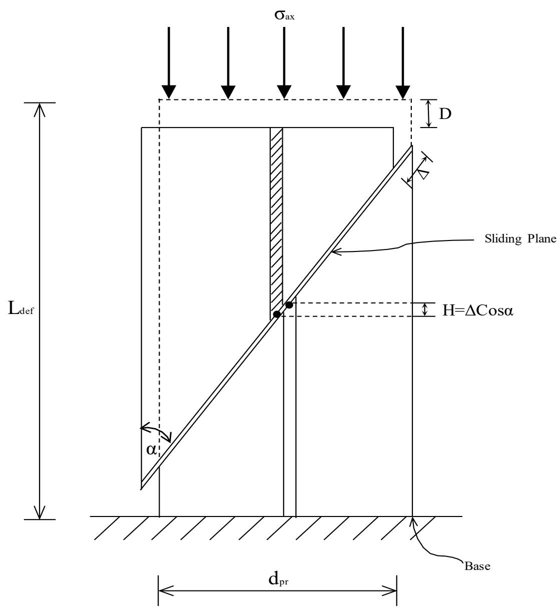


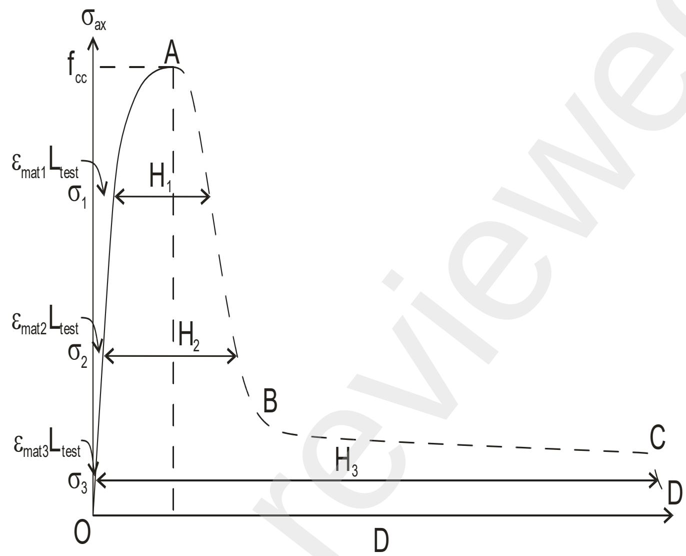


Fig. 3. Compressive deformation of concrete prism Fig. 4. Variation of axial deformation with applied stress

The stress-deflection relationship in Fig. 4 has reached a stage of nonlinearity. Fig. 4 is resulted by the creation of microcracks as a result of the fibers' interaction across the crack, which effectively limits UHPFRC passively. Since microcracking pervades the whole specimen, any non-linearity on the linear part OA can be denoted a material feature. There are three stages defined for material deformation in Fig. 4 as the initial stage ($\varepsilon_{mat2}L_{test}$), post-initial stage ($\varepsilon_{mat1}L_{test}$) and the final stage ($\varepsilon_{mat3}L_{test}$) before first cracking stress ($\sigma_1$), close to ultimate stress ($\sigma_2$) and final (collapse) stress ($\sigma_3$) respectively. Additional loading causes a single sliding plane to form at an angle α in Fig. 3, at the weakest region in the concrete. In the softening region of the stress-deflection correlation in Fig. 4, the axial deformation caused by sliding is taken as H and can be calculated geometrically to determine the full deformation which is,

$$\delta = \varepsilon_{mat}L_{def} + H \qquad (2)$$

As a result, defining the non-material or local deformation (H1, H2, and H3) at various phases of loading with the accompanying stresses, as previously discussed, is required. If the specimen size in Fig. 3 was twice then the total height $L_{def} = 2L_{test}$, the ascending area of the stress-strain behavior stays fixed as this is a size-dependent nature by the equivalent strain owing to sliding H. The development of the material ductility model delineates the behavior into two stages, as shown in Fig. 5.

Stage-1: Strain-based ascending branch material deformation

Stage-2: The material and sliding deformation of the descending branch

The primary method for analyzing the compression failure behavior of structural elements is nonlinear analysis, and the entire stress-strain curve of the unconfined concrete is required for the analysis [40]. Several experiments on UHPFRC have been conducted to determine the global strain, which may subsequently be extracted to generate an analytical formulation [2]. In this regard, none of the existing equations can well estimate the overall stress-strain response of UHPFRC by means of the specimens' global strain ($\varepsilon_{axgl}$) [41]. From global strain ($\varepsilon_{axgl}$), it is possible to comprehend a specimen's size effect on the stress-strain relationship. Chen and Visintin [19] developed an equation for quantifying global strain for unconfined strength concrete from varying specimen sizes,

$$(\varepsilon_{axgl-2})_n = [(\varepsilon_{axgl-1})_n - (\varepsilon_{mat})_n]\frac{L_{pr-1}}{L_{pr-2}} + (\varepsilon_{mat})_n \qquad (3)$$

Where $\varepsilon_{axgl-1}$ is the global strain of a reference specimen of 200 mm and $L_{pr-1}$ is the specific length, $\varepsilon_{mat}$ is the material strain, and $L_{pr-2}$ is the specific length/height of the target specimen. The subscript η is the specimen size factor equivalent to $L_{pr-1}/L_{pr-2}$. This equation can apply to other types of concrete where the material properties, size factor, and global strain characteristics should be consistent with the specified concrete specimen. Fig. 5 illustrates the idealized stress-strain diagram for UHPFRC specimens under uniaxial compressive loads that produce the global strain, which is the function of stress. As can be observed, each specimen has the same material strain up to ($\sigma_s$), and each specimen's ascending branch has a comparable linear slope. The size-effect of the specimen is visualized in the diagram, and it can be seen that as the η decreases, there is a loss in ductility in the descending branch. On the other hand, as the η increases, ductility increases in in the softening zone.

The analytical model proposed by Popovics [28] can output the full stress-strain response of concrete, including both the linear elastic and softening branches with the following equation,

$$f = f_0 \frac{\varepsilon}{\varepsilon_0} \frac{n}{n - 1 + \left( \varepsilon / \varepsilon_0 \right)^2} \tag{4}$$

Where $f$ is the predicted stress at strain $\varepsilon$, $f_0$ is the measured peak strength, $\varepsilon_o$ is the measured strain, and n is the factor controlling ductility. To include size-dependency, Chen, and Visintin [19] suggested a revised value of peak strain ($\varepsilon_{co}$) which was then incorporated in the modified Popovics' model for quantifying the complete stress-strain behavior of the specimen. They used regression analysis on a large number of NSC test data to extract the value of $\varepsilon_{co}$. This adjusted $\varepsilon_{co}$ with the strain-adjustment factor of eq (3) makes the stress-strain relationship completely size-dependent, and this relationship for any specimen size could be enumerated from one size of the specimen. The slenderness factor μ in this equation must be greater than or equal to 2 for consistent natural angel creation in the wedge cracking portion. In light of the adjusted value of $\varepsilon_{co}$, the amended Popovics's formula for the size influences stress-strain response is,

$$f = f_{co} \frac{\left[ \frac{(\varepsilon_{ax})_{pop}}{\varepsilon_{co}} \right] r}{r - 1 + \left[ \frac{(\varepsilon_{ax})_{pop}}{\varepsilon_{co}} \right]^r} \tag{5}$$

where $r$ is an influencing parameter that controls the softening behavior of the concrete, and $r = \frac{E_c}{[E_c - (f_{co}/\varepsilon_{co})]}$. As a result, Popovics' equation produces the influence of size effect in the stress-strain behavior. The influencing elements have then been included to the modified Popovics analytical model to create a size-dependent stress-strain analytical model for UHPFRC.

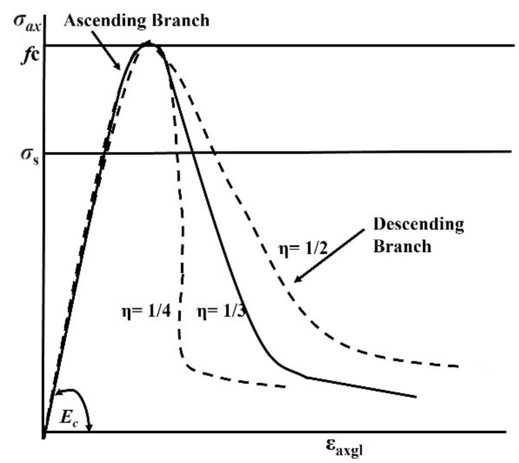


Fig. 5. Idealised size-dependent stress-strain curve for UHPC specimens

### *3.2 Extracting regression for UHPFRC*

For the analytical model, the global strain at peak compressive stress ($f_{co}$) for a standard specimen of length 200 mm, $\varepsilon_{co\text{-}200}$, can be used to create size-dependent characteristics. Peak strain can be transformed into global strain for a reference length of specimen 200 mm by using the strain-adjustment factor proposed by Chen, Visintin [19],

$$\varepsilon_{co-200} = \left(\varepsilon_{co-test} - \frac{f_{co}}{E_c}\right)\frac{L_{pr-test}}{200} + \frac{f_{co}}{E_c} \qquad (6)$$

where, $f_{co}$ = Peak stress, $\varepsilon_{co\text{-}test}$ = Peak strain from the test result, $L_{pr\text{-}test}$ = Test specimen length

$L_{pr}$= Test specimen length

In this paper, authors have done a linear regression on 121 data from published research relevant to the global strain of the specimen at peak stress to determine relationships between $\varepsilon_{co\text{-}200}$ and $f_{co}$.. The authors then separated the test findings into three distinct fiber concentrations, such as 1%, 2%, and 3%, and carried out linear regressions for each fiber concentration using test results of steel fibers with a comparable proportion from published literature. A comprehensive linear regression analysis was performed to establish a correlation between $\varepsilon_{co\text{-}200}$ and $f_{co}$, as presented in Fig. 6, and the following equation is developed for the varying fiber concentrations of UHPFRC:

For 1% fiber, $\varepsilon_{co-200-1} = 6.42 \times 10^{-6} f_{co} + 2.88 \times 10^{-3}$ (7)

For 2% fiber, $\varepsilon_{co-200-2} = -1.78 \times 10^{-6} f_{co} + 3.88 \times 10^{-3}$ (8)

For 3% fiber, $\varepsilon_{co-200-3} = 1.08 \times 10^{-6} f_{co} + 3.44 \times 10^{-3}$ (9)

These equations represent the adjusted $\varepsilon_{co}$ for the standard specimen size of UHPFRC. The size-dependent compressive ductility characteristics of UHPFRC may then be quantified by converting them into other sizes.

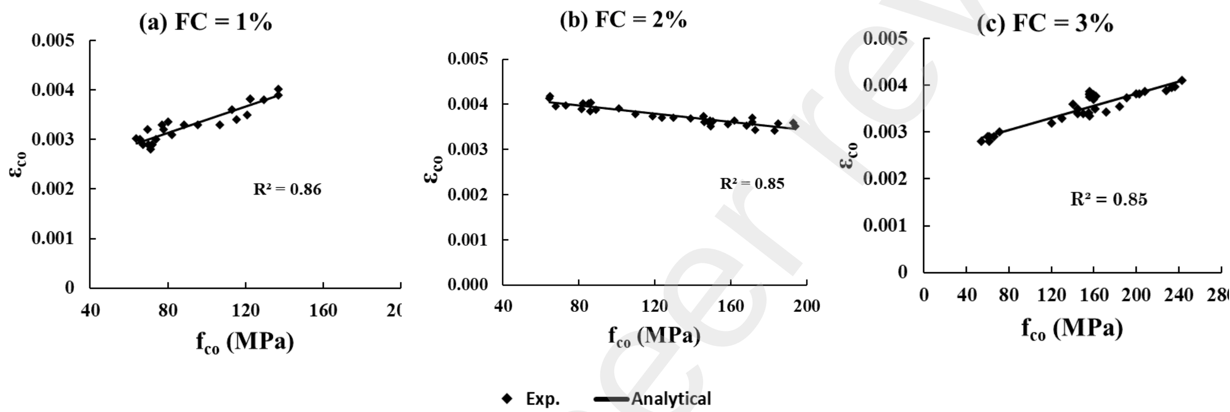


Fig. 6: Regression analysis on the published test data

# 4 Test results and discussion

*4.1 Compressive strength results*

Axial stress-strain responses of UHPFRC consist of peak strength, peak strain, final collapse strength, and strain at different fiber concentrations are provided in Table 3. It is noted that every four specimens were tested for each slenderness factor and fiber concentration to determine the overall stress-strain behavior. In Table 3, it is observed that mean peak strengths showed a very close value to the corresponding specific specimen size with the same fiber concentration. Table 3 exhibits that incorporating higher fiber concentration, the peak strain and final failure strain increased significantly for each specimen size except Exp.100×300-2 and Exp.100×300-3, where the peak strength remained the same. This behavior directly demonstrates that fiber can enhance the ductility behavior of UHPFRC with higher dissipation of energy and higher residual stress rather than NSC agreeing with previous researchers [20].

Table 3: Experimental results

| Specimen Designation | Slenderness Factor | Modulus of Elasticity (MPa) | Peak Mean Strength (MPa) | Standard Deviation, MPa | Peak Strain × $10^{-5}$ | Final Failure Strength (MPa) | Final Failure Strain × $10^{-3}$ |
|---|---|---|---|---|---|---|---|
| Exp.100×200-1 | 2 | 35001 | 137 | 3.37 | 415 | 6.68 | 101 |
| Exp.100×200-2 | 2 | 37246 | 155 | 5.2 | 443 | 4.39 | 148 |
| Exp.100×200-3 | 2 | 37461 | 160 | 1.63 | 451 | 7.23 | 187 |
| Exp.100×300-1 | 3 | 38023 | 124 | 4.97 | 354 | 0.63 | 092 |
| Exp.100×300-2 | 3 | 38962 | 142 | 3.74 | 366 | 2.48 | 110 |
| Exp.100×300-3 | 3 | 40583 | 142 | 1.26 | 370 | 1.47 | 132 |
| Exp.100×400-1 | 4 | 35515 | 140 | 1.83 | 402 | 0.98 | 066 |
| Exp.100×400-2 | 4 | 37279 | 142 | 2.94 | 396 | 1.95 | 080 |
| Exp.100×400-3 | 4 | 34191 | 143 | 3.16 | 438 | 2.82 | 092 |

Specimens with 2% and 3% fiber concentration2%, and 3% fiber concentration exhibited higher failure strength than those with 1% fiber concentration. Exp.100×300-1 and Exp.100×400-1 specimens exhibited the lowest failure strength, while the Exp.100×200-1 showed higher failure strength for a similar fiber concentration. The size effects are apparent from Table 3, as the higher size of the specimen revealed lower failure strength. Moreover, failure strain increases as fiber concentration increases, but it reduces as specimen size increases. Moreover, it is evident that UHPFRC failure strain is substantially larger than that of NSC and HSC. The failure strains for NSC and HSC are close to 0.0035 and 0.006, respectively, but the UHPFRC had the lowest failure strain, which was close to 0.0660. Similar behavior of UHPFRC at the failure stage was observed in the experimental investigation by Lim and Ozbakkaloglu [42]. This behavior suggests that UHPFRC has much greater serviceability than NSC and HSC.

### *4.1 Influence of size-dependency with fiber*

The experimental investigation incorporates the size-dependent stress-strain curves of UHPFRC specimens for different fiber concentrations, summarized as an average of four specimens in Fig. 10. It can be seen from Figs. 10 (a, b, and c) for UHPFRC specimens, ascending branch showed quite similar fashion in nature and looked mostly linear until the peak stress; nevertheless, the softening branch followed the rapid reduction of strength until the stable plateau of stress was achieved, which represents greater overall energy absorption capacity and high ductility capacity [1, 20, 43]. As expected, the higher the fiber concentration in each size group, the higher was the total axial contraction of the specimens with substantial material ductility. This improved ductility is attributed to the steel fibers partially restraining the lateral expansion and preventing uncontrolled sliding with inclined sliding planes consenting for more significant axial contractions. It is also seen that as the slenderness factor of the specimen increases, the post-peak descending branch becomes steeper, showing a snapback phenomenon with brittle behavior of the wedge formation with the specimen length, and size effects are apparent, as illustrated in Figs. 10 (a, b, and c), strongly agrees with the experimental finding by Kazemi and Lubell [20]. It can be noted that the fiber concentrations 2% and 3% exhibited compressive strength up to 155 MPa and 160 MPa for the specimen of slenderness factor 2; consequently, the specimen of slenderness factor 3 and 4 showed quite similar compressive strength behavior. In addition, it can be noticed from Fig. 10 (c) that the size effects of the UHPFRC specimen with 3% fiber concentration exhibited the highest ductility and compressive strength due to the fiber bridging effect, which ensures smaller crack opening and good distribution of fiber during the mix that becomes internal bonding more apparent with concrete.

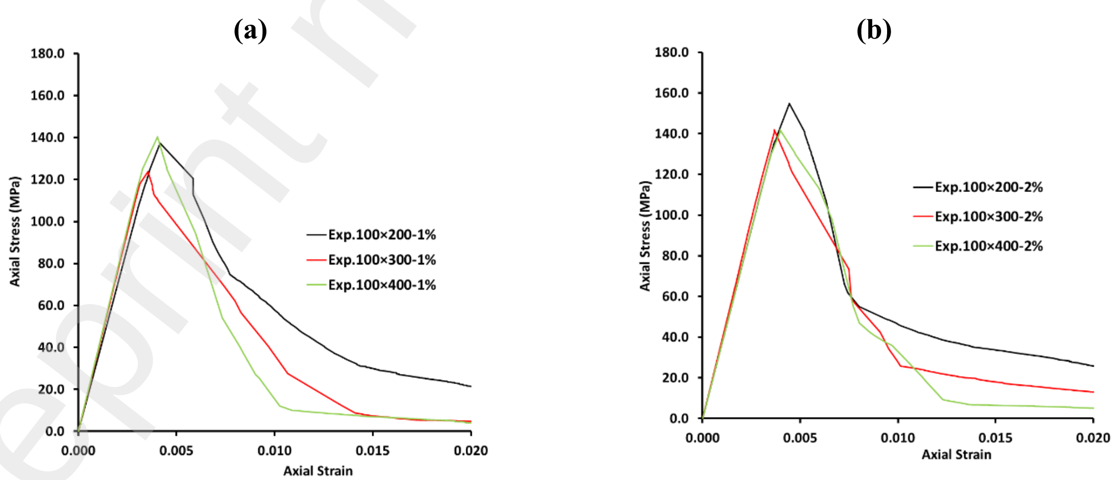

**(c)**

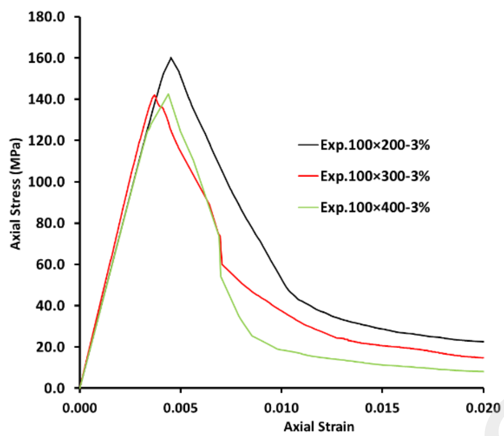


Fig. 10: Stress-strain responses due to different specimen sizes for (a) 1% fiber concentration (b) 2% fiber concentration (c) 3% fiber concentration

### *4.2 Comparison with present test results*

To compute the size-effect response of UHPFRC using the preceding experimental results, the analytical results with slenderness factors 2, 3, and 4 of the specimens with 1% fiber concentration are derived using Eqs. (6) and (7). Similarly, Eqs. (6) and (8) are used for 2%, and Eqs. (6) and (9) are used for 3% fiber concentration. For the analysis, 200 mm length/height of the specimen is considered as the standard size for each 1%, 2%, and 3% fiber concentration, where the $L_{pr\text{-}200}$ is regarded as the platen-to-platen overall contraction and termed as global strain and the conversion procedure of global strain for any other length explained in the earlier section. Then the predicted stress-strain analytical model for fiber concentrations 1%-3% but different specimen sizes are compared against the experimental results as shown in Figs. 11 (a, b, and c), respectively. Examining the size-dependent stress-strain model of UHPFRC, it is manifested that the developed analytical approach is most precise in quantifying the size-dependent compressive ductility responses of the tested specimens, as illustrated in Figs. 11 (a, b, and c). Furthermore, the predicted responses exhibited a very close fit with the experimental investigation during the initial period, where the material exhibited linear behavior up to peak stress. There is an average difference of observed peak stress with slenderness specimen factor 2 yielding 0.34%, 0.26%, and 10.5% between the predicted approach and the test results for fiber concentration 1%, 2%, and 3%, respectively. In addition, the peak stress with slenderness specimen factors 3 and 4 was also observed to be quite similar with varying fiber concentrations. This is particularly evident that the analytical predictions revealed a slightly higher value than the experimental results because the analytical approach is continually developed based on the fundamental assumption criteria. Moreover, the experimental results exhibited lower load capacities due to the formation of wedge after sliding zone and less composite action with weak fibre-interaction effect especially lower fiber concentration leading to larger crack opening that makes the stress at stable plateau condition. In general, it can be concluded that the size effects compressive ductility stress-strain prediction of different slenderness factors of the specimens using the analytical model mentioned in this study provides a conservative estimate of the test results.

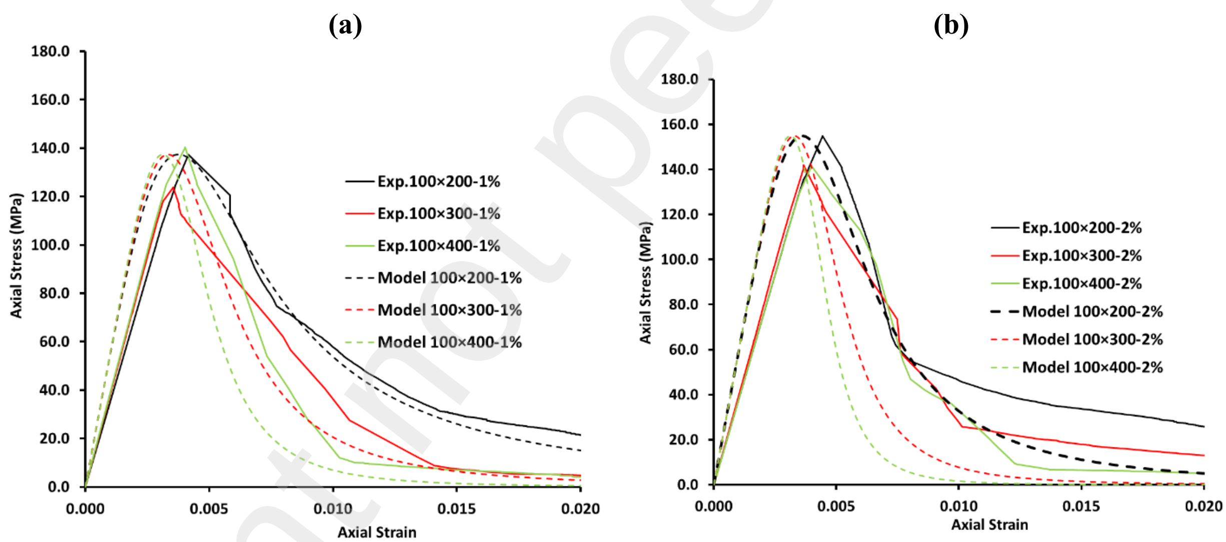

(c)

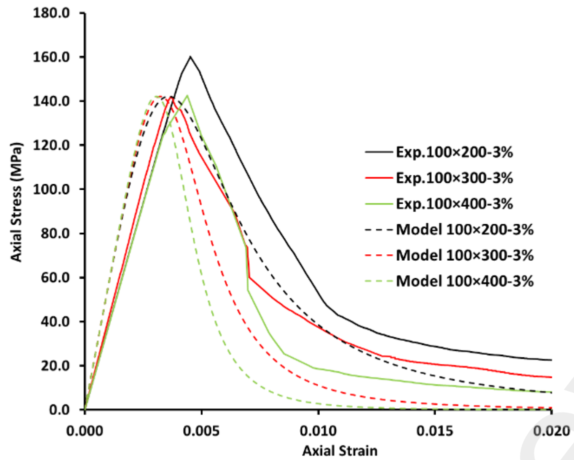


Fig. 11: Comparison with present experimental results with different specimen sizes for (a) 1% fiber concentration (b) 2% fiber concentration (c) 3% fiber concentration

## *4.3 Comparison with published test results*

For validation of the analytical method, several available existing test results databases were incorporated into the method to compare and assess the size-dependent stress-strain behavior of UHPFRC. Numerous published experimental investigations have been done previously on varying specimen sizes with 1%, 2%, and 3% fiber concentrations that accomplished the slenderness factor condition of $\mu >= 2$ [44-48]. The existing test data is compared against analytically predicted curves for incorporating 1%, 2%, and 3% fiber concentration of UHPFRC and plotted in Figs. 12 (a, b, and c), respectively. It can be noted that analytical results are referred to as 'Models' for easy recognition in the plots. All experimental setups followed a slenderness ratio $\mu = 2$, and $L_{pr}$ ranged from 50 mm to 200 mm in length. The respective analytical predictions can be employed using Eq. (4) for these test results, converting the test result for a cylindrical specimen $L_{pr} = 200$ mm.

It can now be noted that the predicted approach gives a closer estimate of the test data, albeit a relatively slight variation observed with few test results. Despite the close fit observed in the linear ascending curves except for 1% fiber concentration, the softening branches of the stress-strain curves can be seen to have scatter results, especially for 1% and 3% fiber concentrations, as depicted in Figs. 12 (a and c). This would suggest that there may be complexity in measuring total dilation due to the formation of the wedge during experimentation. In other means, the highest fiber concentration increased restraint to shrinkage, which leads to an increasing micro-cracking in the concrete at the post-sliding wedge zone. Similarly, the lowest fiber concentration is not effective in holding the fiber bridging effect resulting in a scattered softening response with a weaker bond and large crack opening in the specimen. It should be noted that the analytical model envisages the peak strain slightly lower than the experimental peak strain in the case of 3% fiber concentration; consequently, well agreement was observed between predicted and test peak strain for 1% and 2% fiber concentrations as illustrated in Figs. 12 (a and b). This could happen due to disparate experimental measurement methods for UHPC and irregular fiber matrix distribution in the concrete mixes [49].

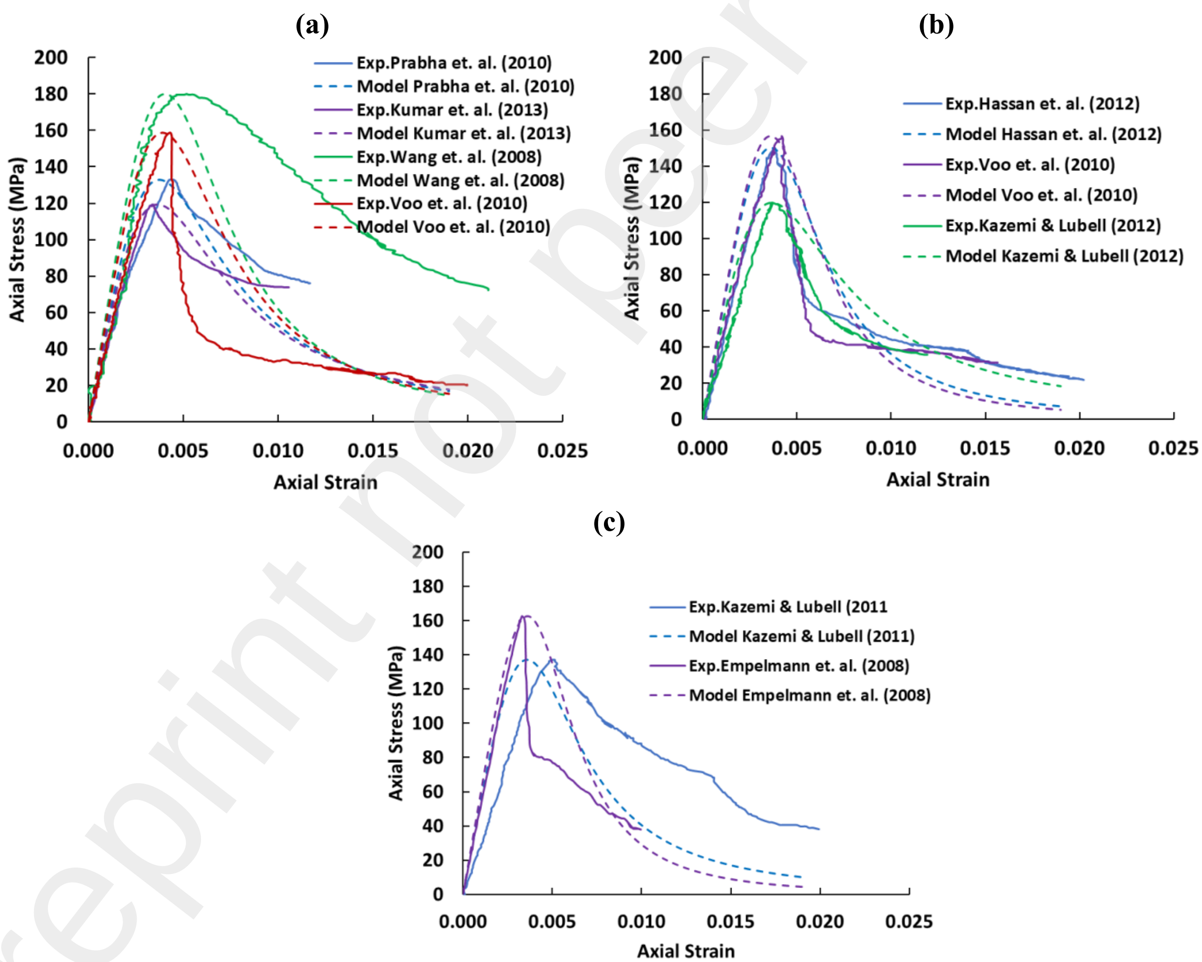

Fig. 12: Comparison with published test results for (a) 1% fiber concentration (b) 2% fiber concentration (c) 3% fiber concentration

Further comparison can be made among the test results on the compressive behaviors of the specimens. Voo and Foster [45] achieved around 145 MPa for a 100 × 200 mm cylinder with 2% fiber concentration, while for the same size and fiber percentage, Kazemi and Lubell [20] achieved around 120 MPa. The model closely predicts similar peak stress for both test data, thus indicating it can be implicated in different experimental measurement techniques. Moreover, the higher residual stress exhibited in the experimental measurements is also predicted conservatively. The models can also accurately predict stable dilation in the softening region up to final failure, which indicates the models can determine the substantial ductility response of UHPFRC. Besides, higher fiber concentration leads to efficient confinement at the stable stress plateau position, which appears to be significant ductility behavior, and it can withstand a more extended period due to high cyclic fatigue loading like earthquakes. Thus, the model can be implemented to provide a long-term warning prior to structural failures, which allows preventive measures for the structures. The analytical model, which takes account of the size effects response, is found to predict the test data better; however, the model shortens the amount of future experimental work necessary for producing an advanced type of UHPC by incorporating varying materials and conventional methods [50].

## 5 Analysis of the deformation-based segmental approach

An effective experimental study has been done to develop a material model that can be used in a numerical model to evaluate the rotational strength of plastic hinges of UHPFRC beam members. Due to the residual stress and tensile strength behavior of concrete, general design and evaluation of reinforced concrete members are based on size-independent strain-based [51-54]. As a result, sizes cannot possibly be introduced. In addition, the moment-curvature approach is unable to account for the creation of wedges during concrete softening, as it does not consider shear friction slip and cannot handle the size-dependency nature of the issue. To overcome the limitations of strain-based methods, a flexural segmental moment-rotation approach has been proposed for analyzing reinforced concrete beams. This method enables the measurement of deformation-based hinge rotation while considering the size-dependent mechanisms [55-58].

The importance of a new type of UHPFRC reflects upon the industrial implication of concrete. To review the implication, the segmental moment-rotation approach is the method that can quantify the complete response of UHPFRC members, especially after cracking stages which provides a large strain capacity. To illustrate the inclusion of UHPFRC in the analysis, let us consider the segment in the constant moment region of the UHPC beam of length $L_{scm}$ as illustrated in Fig.13. The beam length of $L_{scm}$ has consisted of the length $2L_{def}$ in which $L_{def}$ is taken as the length of the softening wedge that can form anywhere of the constant moment region, but for simplification of the analysis, it is considered symmetric about the centerline of the segment [59]. It is important to define the baseline (A, B), datum (E), and half the length $L_{def}$ from A to E when conducting the analysis due to its symmetrical nature.

The numerical analysis has been performed to quantify the moment (M) for a given imposed end rotation ($\theta$) and Euler-Bernoulli linear displacement at both ends of the segment in order to extract the differences of rotation with that applied moment which depends on the length of softening wedge $L_{def}$ which is size-dependent as depicted in Fig. 13. In the region of concrete softening, the length $L_{def}$ can be any size. However, it is appropriate to choose a length that corresponds to a multiple of the crack spacing of the segment in the area of constant moment. [60]. The corresponding top concrete face deformation ($\delta_{top}$) is guessed for the known rotation, thus defining the neutral axis depth ($d_n$).

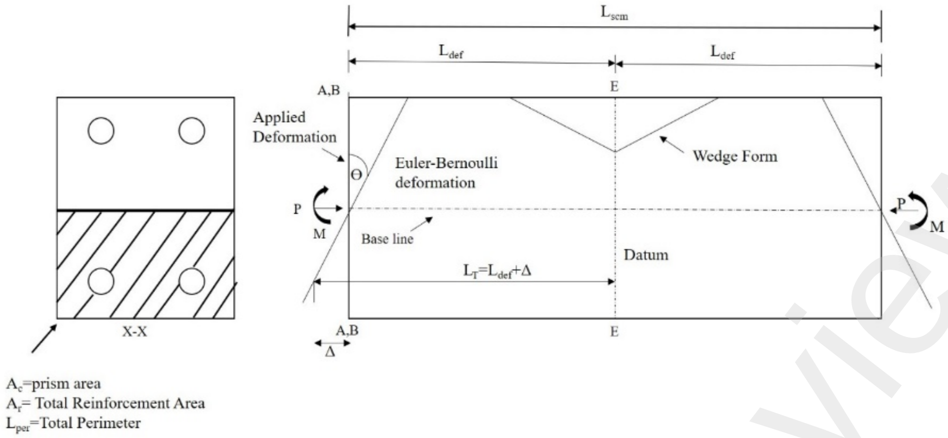


Fig. 13: Deformation-based segmental moment-rotation approach

The effective strain (ε) in the uncracked region is obtained by dividing the deformation A-A to B-B in Fig. 14 by the half beam segment length $L_{def}$. This is necessary to obtain the deformation (A-A to B-B) in the uncracked region.

By utilizing a size effect compressive stress-strain relationship, where $L_{def}$ is considered as the cylinder height, it is possible to compute the stress (σ), strain (ε), and force (F) in the concrete as shown in Fig. 14. The corresponding stress (σ) and force (F) can be calculated based on the stress-strain behavior for the reinforcing bars. The force in the reinforcement can be quantified by using well-established partial interaction theory at the serviceability limit state [59, 61-63] that is, the interfacial bond involving the steel bar and the surrounded concrete at the tension zone, referred to as tension stiffening phenomenon [58, 64]. In UHPFRC, when determining the ultimate hinge rotation, crack widths often become significant as tension stiffening plays a minor role. Consequently, steel is not explicitly allowed for tension stiffening. Once the internal forces (F) in Fig. 14 have been defined, they can be added to determine whether $\delta_{top}$ equilibrium was attained for the given guess. If it is the ultimate moment corresponding to the rotation capacity, $\theta$ can be predicted; if not, the estimate $\delta_{top}$ can be conformed until the equation reaches an equilibrium condition.

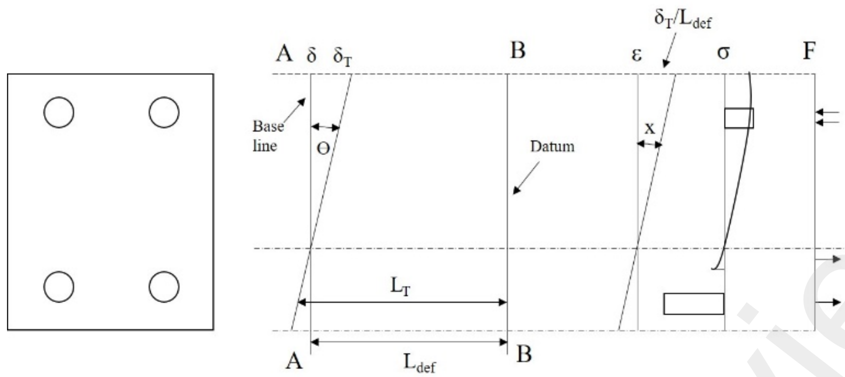


Fig. 14: Deformation-based segmental moment-rotation approach for half section

## 6 Application of segmental analysis for UHPFRC beams

As an example of applying the bending numerical segmental moment rotational approach, consider a UHPFRC beam member with dimensions of 150 × 350 mm with an effective depth of beam 314 mm and reinforced with steel reinforcing bars of 3-16 mm diameter in the soffit area and bars of 2 – 10 mm diameter in the compression area of the beam. In the intended model, the steel reinforcement is assumed to be elastic and perfectly plastic, with a yield strength of 450 MPa. To evaluate the flexural ductility/rotational capacity of the reinforced UHPFRC beam element, the analysis considers the impact of fibers and UHPFRC concentration.

### *6.1 Influence of size factor*

To extrapolate the experimental data from the laboratory to field scale level, comprehending the influence of specimen slenderness factor obtained directly from the test results and then incorporating those properties in the numerical segmental moment-rotation method to predict the structural behavior of UHPFRC beam, which is quite realistic in terms of ductility. The moment-rotation behavior of reinforced concrete UHPFRC beam element incorporating the size-dependent stress-strain responses of the varying UHPFRC specimens with fiber concentrations of 1, 2, and 3% are quantified as shown in Figs—15 (a, b, and c). In addition, the moment-rotation responses of the beam were subsequently converted to moment-curvature by dividing the abscissa (rotation) in Figs. 15 (a, b, and c) by $L_{def}$ as illustrated in Figs. 15 (d, e, and f) could be used directly to obtain the disparity in flexural rigidity (EI) along with the moment, as depicted in Figs. 15 (g, h, and i).

These relationships from the model can next be employed to evaluate a UHPFRC member element over the full length, including the softening region with higher ductility of UHPC.

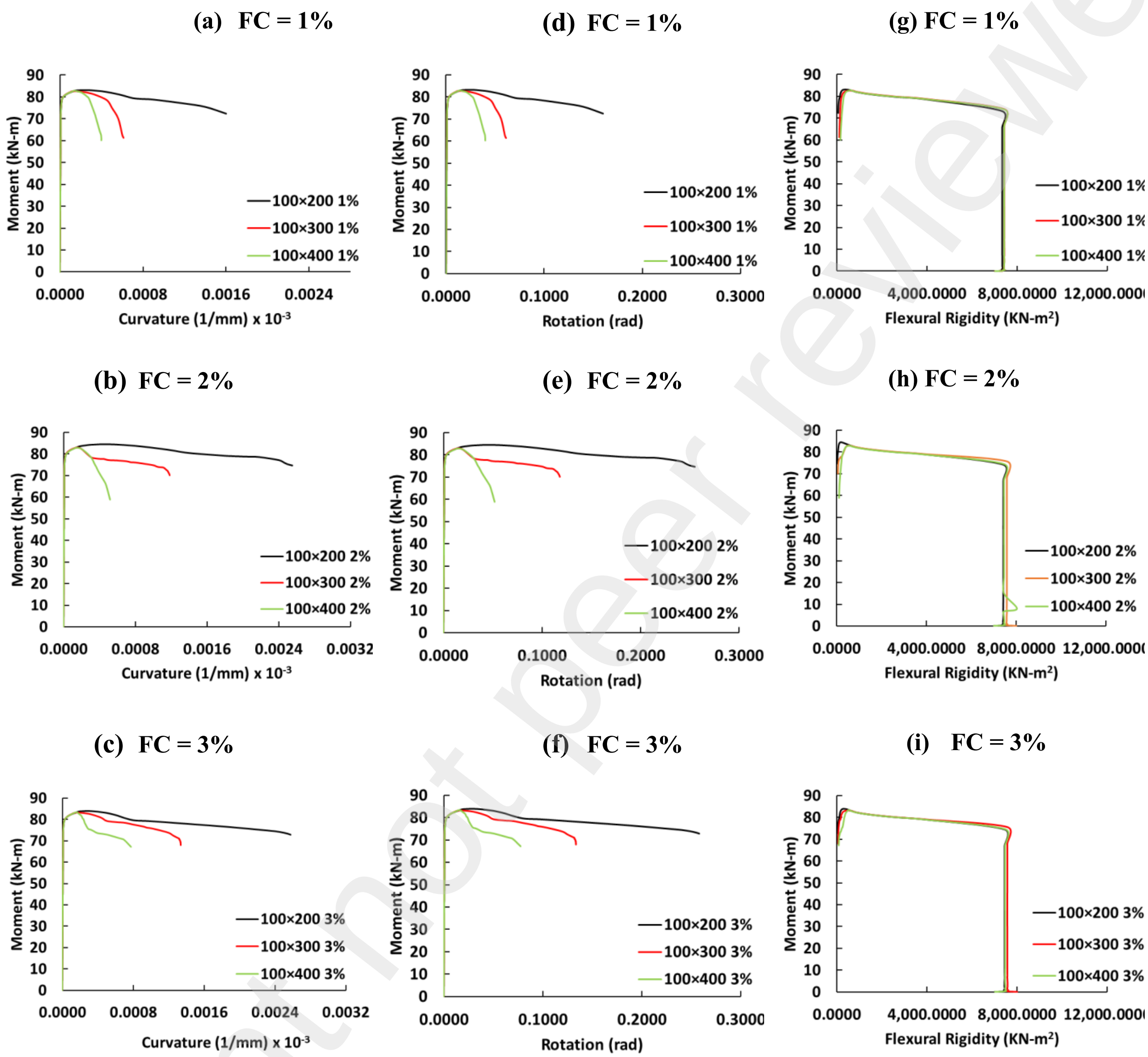


Fig. 15: Influence of fiber on moment versus rotation, curvature, and flexural rigidity for UHPFRC beam

It is interesting to note from all of the Figs. 15 (a-i) that as specimen size or slenderness increases, the UHPFRC beams exhibit snapback or become more brittle, and the phenomenon of size effects is amply illustrated, particularly on the moment-rotation and moment-curvature curves. This intrinsic behavior was mentioned by the additional researcher as well [20, 65, 66]. For instance, by reducing the specimen size, the rotation capacity of the UHPFRC beam in the post-peak softening region was improved; however, the slope decreases as the specimen size decreases. Notably, the ductility/rotation capacity of the beam increased apparently as the size factor (η) of the specimen increased, while the opposite phenomenon is true when the η value reduces, as shown in Figs. 15 (a-i). Post-peak behavior from the moment-curvature curves shows the ductile behavior of UHPFRC which follows a similar pattern for RC beams to exhibit ductility [67, 68]. The specimen sizes noticeably affect the post-peak descending branch slope of the beam. In contrast, the initial slope of beam curves is insignificantly influenced regardless of the specimen size factor. Similar behavior was observed experimentally for UHPC beams by Yoo and Yoon [65]. This predominant behavior is consistent with the finding of Fantilli et al [66] that the softening strain of the RC beam exhibited a marginal size effect. This result shows a direct agreement of the UHPFRC beam in the descending branches, which is size-dependent as they can be attributed to the wedge formation at an early age during testing.

### 6.2 *Influence of steel fiber concentration*

The rotation of reinforced concrete UHPFRC beam, including varying specimens' stress-strain material properties, is compared according to the different fiber concentrations and the specimen slenderness factor (e.g. $\mu$ = 2, 3, and 4) as depicted in Figs. 16 (a-i). In the analysis, moment-rotation responses are always size-dependent, which allows the deformation. Similarly, the transformation of moment-rotation to moment-curvature and then moment-flexural rigidity (EI) is also influenced by the size-dependency factor as shown in Figs. 16 (d-f) and Figs. 16 (g-i).

**(a) μ = 2** **(d) μ =2** **(g) μ = 2**

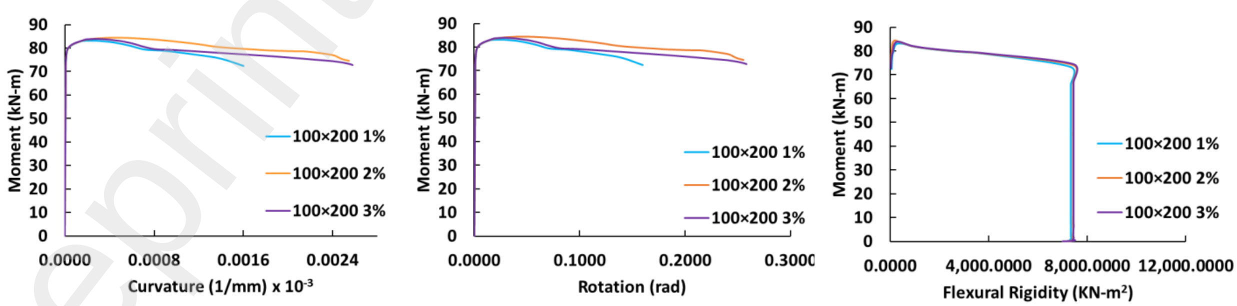


**(b) μ = 3** **(e) μ = 3** **(h) μ = 3**

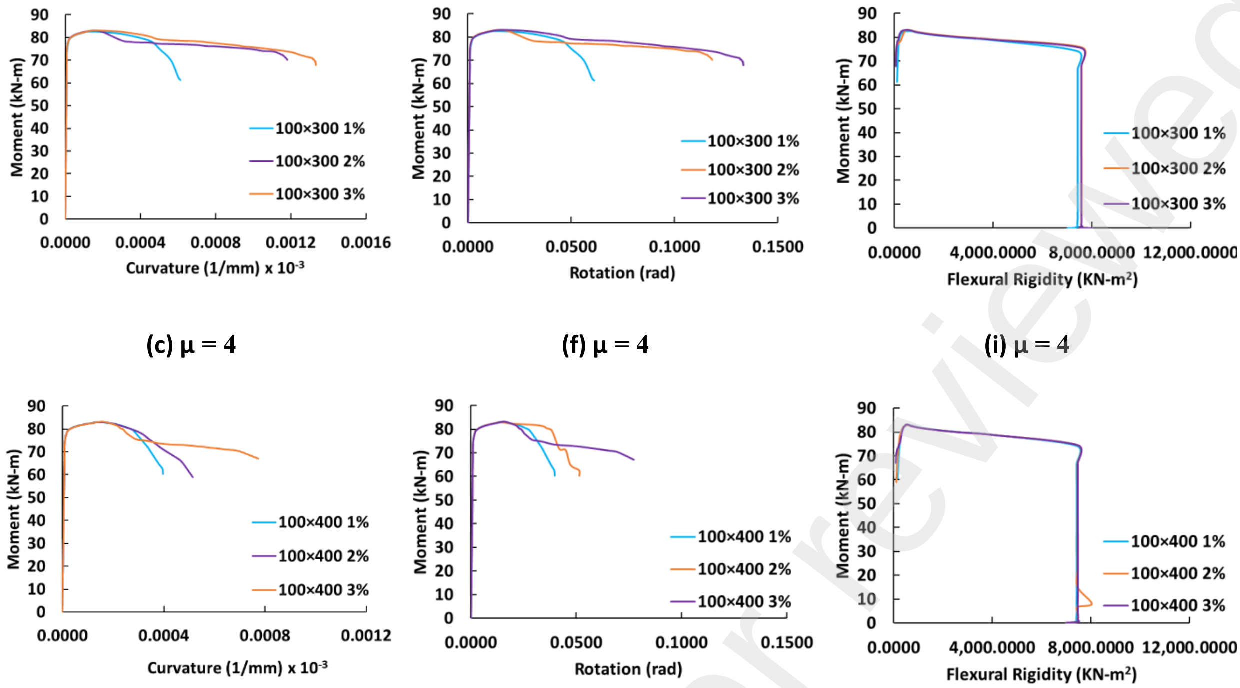


Fig. 16: Influence of size on moment versus rotation, curvature, and flexural rigidity of UHPFRC beam

It is seen that UHPFRC beams exhibited a more significant increase in rotation and curvature with the contribution of varying steel fiber concentration in ductile post-peak behavior, as illustrated in Figs. 16 (a-c) and Figs. 16 (d-f); however, the flexural rigidity shows insignificant changes in the softening stages of the beam. Regardless of the fiber concentration, the initial slope of the ascending stage of the diagram appears to be linear elastic; consequently, the slope of the descending branch decreases as fiber concentration increases. The intrinsic behavior strongly agrees with the finding observed in the test results [20,65]. In addition, the lowest steel fiber concentration evinced the lowest rotation for UHPFRC beams observed after the post-peak region. In contrast, the highest-fiber concentration shows higher rotation employing greater ductility response with high energy absorption capacity. This predominantly response leads to the steel fiber bridging effect during cracking that partially restrained the lateral amplification and allowed more significant axial contraction. It is seen from Figs. 16 (a, b, and c) that the rotation capacities are decreased by about 62% and 75% for the specimen slenderness factors of $\mu$ = 3 and 4, compared to the reference specimen slenderness factor ($\mu$ = 2) for the fiber concentration 1%. For 2% fiber concentration, 54%, and 80% decrease in the rotation capacities for the same instant of slenderness factor can be observed in Figs. 16 (a, b, and c). Finally, for 3% fiber concentration, the rotation capacities decreased by 49% and 70% as illustrated in Figs. 16 (a, b, and c). In Figs. 16 (d-f), a similar observation is found for curvature behavior with the corresponding specimen slenderness factors with regard to reference, as mentioned earlier for the fiber concentrations 1%, 2%, and 3%. It can be understood that the greater the slenderness factor, the more significant the reduction of rotation/curvature capacity of the UHPFRC beam compared to the standard size of the specimen where the $L_{def}$ is defined as 200 mm length in the wedge formation in the sliding zone of the beam. In other words, higher fiber concentration demonstrates higher rotation/curvature capacity of beam element, which can be attributed to the strong fiber-bridging effect, good bond characteristics of concrete, and smaller crack opening. Due to the impact of different fiber concentrations, it is revealed that the ultimate moment capacity is quite similar.

## 7 Conclusions

First, an experimental investigation was conducted out to quantify the size effects of compressive ductility responses of UHPFRC under uniaxial compression with varying fiber concentrations based on one standard size of specimen test to derive any sizes. Then the size effects on the stress-strain behavior is incorporated into the numerical flexural numerical segmental approach to simulate the rotation of the plastic hinge of the UHPFRC beam. Based on the research presented here, it can be drawn the following conclusions: -

i. The compressive ductility of the UHPHFRC specimen exhibited a relatively brittle nature in the load-carrying capacity as the slenderness factor of the specimen increased, which can be explained as a rapid reduction of specimen capacity due to the formation of wedges along the length of the specimens, indistinguishable in RC element which implies clear size-effect highly apparent to UHPFRC specimens.

ii. UHPFRC specimens of smaller slenderness factors tend to show minor improvement of compressive strength, indicating specimen size effects on the improvement of strength of UHPFRC being modest.

iii. The addition of varying fiber concentrations increased the compressive ductility of UHPFRC, leading to a considerable increase in energy absorption capacity and as a result, ductility proportionately more influential in specimens with lower slenderness factor and higher fiber concentration. The inclusion of fibers insignificantly affected the compressive behavior of UHPFRC, which indicates the fiber is less sensitive to the increase in strength. This higher ductility characteristic should help the significant expansion of UHPFRC to ensure ample warning before the failure of the structure, which can be harnessed to measure the structure due to high-cyclic, seismic and blast loads.

iv. The analytical model was developed to quantify the complete size-dependent stress-strain behavior of UHPFRC, which exploits the relationship between global peak strain ($\varepsilon_{co}$) and peak stress ($f_{co}$) corresponding to the varying fiber concentrations. The analytical size-dependent model of UHPFRC for each fiber concentration agrees well with this study's test results; however, model presents reasonably good prediction with other published test data. This should help further refine the model, allowing full exploitation of the engineering properties of UHPFRC to optimize the design and reduce the cost of experimentation required when extrapolating the outcomes from laboratory to real structures.

v. The numerical flexural segmental method can quantify the ductility/rotation capacity of the UHPFRC beam due to the variation of fiber concentration and specimen size factor at all stages of loading. The approach has shown that RC beams' substantial flexural rotation/ductility capacity has been achieved particularly at higher fiber concentration; however, it predominantly decreased when the specimen size factor decreased, which could be explicated as a reduced capability of larger structures to allow wedge formations.

vi. The analysis did not consider tension stiffening, as crack widths are usually wide in UHPFRC and hence tension stiffening has a negligible effect. However, it would be valuable to investigate the size effects response of RC beams, including the tension stiffening effect, in future studies. In this study, the size effects phenomenon is not presently investigated experimentally; it is desirable that future work involves analysing the flexural behavior of UHPFRC members and its size-dependency with varying fiber type and higher fiber concentration.

**Acknowledgment**

The experimental part of the work has been financially supported by the Australian Government Department of Defense's ''Defense Science and Technology Organization," and the authors wish to acknowledge them. The work was carried out at the Chapman Laboratory of the School of Civil, Environment and Mining Engineering, The University of Adelaide, Adelaide, South Australia, 5005 Australia and the authors would like to thank the technicians in the laboratory for their generous contributions in the experimental works. The numerical modeling portion of the research was conducted on the high-speed computer in the BIM laboratory in the Department of Building Engineering and Construction Management at Khulna University of Engineering and Technology, Khulna -9203, Bangladesh.

**Data Availability Statement**

Upon reasonable request, the corresponding author will make available the data, models, and/or codes used in this study.

**References**

1. Sobuz, H.R., et al., *Manufacturing ultra-high performance concrete utilising conventional materials and production methods.* Construction and Building Materials, 2016. **111**: p. 251-261.
2. Shafieifar, M., M. Farzad, and A. Azizinamini, *Experimental and numerical study on mechanical properties of Ultra High Performance Concrete (UHPC).* Construction and Building Materials, 2017. **156**: p. 402-411.
3. Richard, P. and M. Cheyrezy, *Composition of reactive powder concretes.* Cement and Concrete Research, 1995. **25**(7): p. 1501-1511.
4. Graybeal, B. and M. Davis, *Cylinder or cube: strength testing of 80 to 200 MPa (11.6 to 29 ksi) ultra-high-performance fiber-reinforced concrete.* ACI Materials Journal, 2008. **105**(6): p. 603-609.
5. Graybeal, B.A., *Compressive behavior of ultra-high-performance fiber-reinforced concrete.* ACI Materials Journal, 2007. **104**(2): p. 146.
6. Wille, K., A.E. Naaman, and G.J. Parra-Montesinos, *Ultra-high performance concrete with compressive strength exceeding 150 MPa (22 ksi): A simpler way.* ACI Materials Journal, 2011. **108**(1).

7. Hung, C.-C. and C.-Y. Chueh, *Cyclic behavior of UHPFRC flexural members reinforced with high-strength steel rebar.* Engineering Structures, 2016. **122**: p. 108-120.
8. Ragalwar, K., et al., *On enhancing the mechanical behavior of ultra-high performance concrete through multi-scale fiber reinforcement.* Cement and Concrete Composites, 2020. **105**: p. 103422.
9. Sturm, A.B., P. Visintin, and D.J. Oehlers, *Blending fibres to enhance the flexural properties of UHPFRC beams.* Construction and Building Materials, 2020. **244**: p. 118328.
10. Cadoni, E., et al., *Experimental study on direct tensile behaviour of UHPFRC under high strain-rates.* Construction and Building Materials, 2019. **218**: p. 667-680.
11. Song, Q., et al., *Key parameters in optimizing fibres orientation and distribution for Ultra-High Performance Fibre Reinforced Concrete (UHPFRC).* Construction and Building Materials, 2018. **188**: p. 17-27.
12. Yoo, D.-Y. and N. Banthia, *Mechanical and structural behaviors of ultra-high-performance fiber-reinforced concrete subjected to impact and blast.* Construction and Building Materials, 2017. **149**: p. 416-431.
13. Wille, K., A. Naaman, and S. El-Tawil, *Optimizing ultra-high-performance fiber-reinforced concrete.* Concrete International, 2011. **33**: p. 35-41.
14. Wille, K., S. El-Tawil, and A.E. Naaman, *Properties of strain hardening ultra high performance fiber reinforced concrete (UHP-FRC) under direct tensile loading.* Cement and Concrete Composites, 2014. **48**: p. 53-66.
15. Hassan, A., S. Jones, and G. Mahmud, *Experimental test methods to determine the uniaxial tensile and compressive behaviour of ultra high performance fibre reinforced concrete (UHPFRC).* Construction and Building Materials, 2012. **37**: p. 874-882.
16. Prabha, S.L., et al., *Study on Stress-Strain Properties of Reactive Powder Concrete under Uniaxial Compression.* International Journal of Engineering Science and Technology, 2010. **2**(11): p. 6408-6416.
17. Kazemi, S. and A.S. Lubell, *Influence of Specimen Size and Fiber Content on Mechanical Properties of Ultra-High-Performance Fiber-Reinforced Concrete.* ACI Materials Journal, 2012. **109**(6).
18. Markeset, G. and A. Hillerborg, *Softening of concrete in compression — Localization and size effects.* Cement and Concrete Research, 1995. **25**(4): p. 702-708.
19. Chen, Y., et al., *Size-Dependent Stress-Strain Model for Unconfined Concrete.* Journal of Structural Engineering, 2014. **140**(4).
20. Kazemi, S. and A. Lubell, *Influence of Specimen Size and Fiber Content on Mechanical Properties of Ultra-High-Performance Fiber-Reinforced Concrete.* Aci Materials Journal, 2012. **109**: p. 675-684.
21. Kazemi, S. and A. Lubell, *Size effects on the mechanical properties of UHPFRC.* Proceedings, Annual Conference - Canadian Society for Civil Engineering, 2011. **2**: p. 1256-1265.
22. Reda, M.M., N.G. Shrive, and J.E. Gillott. *Microstructural investigation of innovative UHPC.*
23. Habil, M., et al., *Ultra-high performance concrete: Perspective for the precast concrete industry.* Betonwerk und Fertigteil-Technik/Concrete Precasting Plant and Technology, 2003. **69**: p. 16-29.
24. Yi, N.-H., et al., *Blast-resistant characteristics of ultra-high strength concrete and reactive powder concrete.* Construction and Building Materials, 2012. **28**(1): p. 694-707.
25. B. Frettlöhr, K.-H.R., H. -W. Reinhardt, *Size and Shape Effect of UHPFRC Prisms Tested under Axial Tension and Bending*, in *Bond Behavior of Textile Reinforcements - Development of a Pull-Out Test and Modeling of the Respective Bond versus Slip Relation* 2012, 2211-0844.
26. Graybeal, B., *Material Property Characterization of Ultra-High Performance Concrete*. 2006. 1-176.
27. Maher KT, V.Y., *Taking Ultra-High Performance Concrete to New Height – The Malaysian Experience.* Aspire the Concrete Bridge Magazine, 2016. **Summer 2016**: p. 36-38.

28. Popovics, S., *A numerical approach to the complete stress-strain curve of concrete.* Cement and Concrete Research, 1973. **3**: p. 583-599.
29. Ayub, T., *Stress-Strain Response of High Strength Concrete and Application of the Existing Models*. Vol. 8. 2014. 1174-1190.
30. Mansur, M.A., M. Chin, and T. Wee, *Stress-Strain Relationship of High-Strength Fiber Concrete in Compression.* Journal of Materials in Civil Engineering - J MATER CIVIL ENG, 1999. **11**.
31. Oehlers, D.J., et al., *Simulating reinforced concrete members. Part 1: partial interaction properties.* Proceedings of the Institution of Civil Engineers - Structures and Buildings, 2014. **167**(11): p. 646-653.
32. Bigaj, A. and J. Walraven. *Size effects in plastic hinges of reinforced concrete members*. in *Heron, Vol. 47 (2002) No. 2, pp. 79-80*. 2002. Delft University of Technology.
33. Carpinteri, A., et al., *A numerical approach to modelling size effects on the flexural ductility of RC beams.* Materials and Structures, 2009. **42**(10): p. 1353-1367.
34. Hillerborg, A., *Fracture mechanics concepts applied to moment capacity and rotational capacity of reinforced concrete beams.* Engineering Fracture Mechanics, 1990. **35**(1-3): p. 233-240.
35. Yang, I.H., C. Joh, and B.-S. Kim, *Structural behavior of ultra high performance concrete beams subjected to bending.* Engineering Structures, 2010. **32**(11): p. 3478-3487.
36. Fantilli, A.P., I. Iori, and P. Vallini, *Size effect of compressed concrete in four point bending RC beams.* Engineering Fracture Mechanics, 2007. **74**(1): p. 97-108.
37. Oehlers, D., et al., *FRP-Reinforced Concrete Beams: Unified Approach Based on IC Theory.* Journal of Composites for Construction, 2011. **15**: p. 293-303.
38. ASTM C31, *C31M (2003) Standard practice for making and curing concrete test specimens in the field*, in *West Conshohocken, PA*.
39. ASTM C39. *39/C39M-03 (2003),"Standard Test Method for Compressive Strength of Cylindrical Concrete Specimens"*. in *American Society for Testing and Materials*.
40. Zhao-Hui Lu and Yan-Gang Zhao, M.A., *Empirical Stress-Strain Model for Unconfined High-Strength Concrete under Uniaxial Compression.* JOURNAL OF MATERIALS IN CIVIL ENGINEERING © ASCE, 2010. **22(11)**: p. 1181-1186.
41. Graybeal, B.A., *Compressive Behavior of Ultra-High-Performance Fiber-Reinforced Concrete.* ACI Materials Journal, 2007. **104**(2).
42. Lim, J.C. and T. Ozbakkaloglu, *Stress-Strain Model for Normal- and Light-Weight Concretes under Uniaxial and Triaxial Compression.* Construction and Building Materials, 2014. **71**.
43. Orgass, M. and Y. Klug. *Fibre reinforced ultra-high strength concretes*. in *Proceedings of the International Symposium on ultra-High Performance Concrete, Kassel, Germany*. 2004.
44. Wang, Y., et al., *Experimental and numerical studies on dynamic compressive behavior of reactive powder concretes.* Acta Mechanica Solida Sinica, 2008. **21**(5): p. 420-430.
45. Voo, Y.L. and S.J. Foster, *Characteristics of ultra-high performance 'ductile' concrete and its impact on sustainable construction.* The IES Journal Part A: Civil & Structural Engineering, 2010. **3**(3): p. 168-187.
46. Lavanya, S., et al., *STUDY ON STRESS-STRAIN PROPERTIES OF REACTIVE POWDER CONCRETE UNDER UNIAXIAL COMPRESSION.* International Journal of Engineering Science and Technology, 2010. **2**.
47. Kumar, A.M.U., A.U. Rao, and N. Sabhahit, *Reactive Powder Concrete Properties with Cement Replacement Using Waste Material.* International Journal of Scientific & Engineering Research, 2013. **04**(05).
48. Prem, P., B. Bharatkumar, and N. Iyer, *Mechanical Properties of Ultra High Performance Concrete*. 2012.

49. Abbas, S., M.L. Nehdi, and M.A. Saleem, *Ultra-High Performance Concrete: Mechanical Performance, Durability, Sustainability and Implementation Challenges.* International Journal of Concrete Structures and Materials, 2016. **10**(3): p. 271-295.
50. Zhu, Y., Y. Zhang, and J. Shi, *Finite element analysis of flexural behavior of precast segmental UHPC beams with prestressed bolted hybrid joints.* Engineering Structures, 2021. **238**: p. 111492.
51. Ali, M.S.M., D.J. Oehlers, and M.C. Griffith, *The Residual Strength of Confined Concrete.* Advances in Structural Engineering, 2010. **13**(4): p. 603-618.
52. Bischoff, P., *Tension Stiffening and Cracking of Steel Fiber-Reinforced Concrete.* Journal of Materials in Civil Engineering - J MATER CIVIL ENG, 2003. **15**.
53. Sturm, A.B., P. Visintin, and D.J. Oehlers, *Time-dependent serviceability behavior of reinforced concrete beams: Partial interaction tension stiffening mechanics.* Structural Concrete, 2018. **19**(2): p. 508-523.
54. Sturm, A., P. Visintin, and D. Oehlers, *BLENDING FIBRES TO ENHANCE THE FLEXURAL PROPERTIES OF UHPFRC BEAMS.* Construction and Building Materials, 2020. **244**.
55. Visintin, P., et al., *A Mechanics Based Hinge Analysis for Reinforced Concrete Columns*. Vol. 139. 2013. 1973-1980.
56. Visintin, P., et al., *A mechanics solution for hinges in RC beams with multiple cracks*. Vol. 36. 2012. 61–69.
57. Visintin, P., et al., *The reinforcement contribution to the cyclic behaviour of reinforced concrete beam hinges*. Vol. 41. 2012.
58. Haskett, et al., *Influence of bond on the hinge rotation of FRP plated beams.* Advances in Structural Engineering, 2009. **12**(6): p. 833-843.
59. Visintin, P., et al., *A mechanics solution for hinges in RC beams with multiple cracks.* Engineering Structures, 2012. **36**: p. 61-69.
60. Visintin, P., et al., *A mechanics solution for hinges in RC beams with multiple cracks.* Engineering Structures, 2012. **36**: p. 61–69.
61. Oehlers, D., et al., *FRP-Reinforced Concrete Beams: Unified Approach Based on IC Theory.* Journal of Composites for Construction, 2011. **15**(3): p. 293-303.
62. Seracino, R., D.J. Oehlers, and M.F. Yeo, *Partial-interaction fatigue assessment of stud shear connectors in composite bridge beams.* Structural Engineering and Mechanics, 2002. **13**(4): p. 455-464.
63. Wu, Y., D. Oehlers, and M. Griffith, *PARTIAL-INTERACTION ANALYSIS OF COMPOSITE BEAM/COLUMN MEMBERS*.* Mechanics of Structures and Machines, 2002. **30**(3): p. 309-332.
64. Muhamad, R., et al., *Load-slip relationship of tension reinforcement in reinforced concrete members.* Engineering Structures, 2011. **33**(4): p. 1098-1106.
65. Yoo, D.-Y. and Y.-S. Yoon, *A Review on Structural Behavior, Design, and Application of Ultra-High-Performance Fiber-Reinforced Concrete.* International Journal of Concrete Structures and Materials, 2016. **10**(2): p. 125-142.
66. Fantilli, A.P., I. Iori, and P. Vallini, *Size effect of compressed concrete in four point bending RC beams.* Engineering Fracture Mechanics, 2007. **74**(1-2): p. 97-108.
67. Kheyroddin, A., S. Rouhi, and H. Dabiri, *An experimental study on the influence of incorporating lap or forging (GPW) splices on the cyclic performance of RC columns.* Engineering Structures, 2021. **241**: p. 112434.
68. Li, B., et al., *Experimental investigation on reinforced concrete interior beam–column joints rehabilitated by ferrocement jackets.* Engineering Structures, 2013. **56**: p. 897-909.